[9] J. D. Colby, "Topographic normalization in rugged terrain," *Photogramm. Eng. Remote Sens.*, vol. 57, pp. 531–537, May 1991.
[10] P. S. Chavez, Jr., "An improved dark object subtraction technique for atmospheric scattering correction of multispectral data," *Remote Sens. Environ.*, vol. 24, pp. 459–479, 1988.

Using Temporal Averaging to Decouple Annual and Nonannual Information in AVHRR NDVI Time Series

Jude H. Kastens, Mark E. Jakubauskas, and David E. Lerner

***Abstract*—As regularly spaced time series imagery becomes more prevalent in the remote sensing community, monitoring these data for temporal consistency will become an increasingly important problem. Long-term trends must be identified, and it must be determined if such trends correspond to true changes in reflectance characteristics of the study area (natural), or if their source is a signal collection and/or processing artifact that can be identified and corrected in the data (artificial). Spectrally invariant targets (SITs) are typically used for sensor calibration and data consistency checks. Unfortunately, such targets are not always available in study regions. The temporal averaging technique described in this research can be used to determine the presence of artificial interannual value drift in any region possessing multiyear regularly sampled time series remotely sensed imagery. Further, this approach is objective and does not require the prior identification of a SIT within the region of study. Using biweekly Advanced Very High Resolution Radiometer (AVHRR) normalized difference vegetation index (NDVI) data from 1990 to 2001 covering the conterminous United States, an interannual trend present in the entire scene was identified using the proposed technique and found to correspond extremely well with interannual trends identified using two SITs within the region.**

***Index Terms*—Interannual variability, invariant target, normalized difference vegetation index (NDVI), remote sensing, sensor drift, temporal averaging.**

I. Introduction

PREVIOUS approaches to satellite sensor calibration and drift detection have relied on deriving and applying corrections obtained from geographically specific local targets assumed to be spectrally and temporally invariant, i.e., do not exhibit significant or detectable changes in spectral reflectance characteristics over time [1]–[4]. Typically, these targets are desert or barren lands, such as White Sands Missile Range in New Mexico [1]–[6] or the salt flats of western Utah. In midlatitude regions, however, an appropriate invariant target for scene normalization or detection of sensor drift may not exist or cannot be reliably identified, particularly for coarse-resolution satellite imagery.

Our objective is to derive a methodology for detection and quantification of sensor drift that does not use spectrally invariant targets, but instead defines and uses *annually invariant* targets. We define annually invariant targets as areas exhibiting a highly regular seasonal pattern of normalized difference vegetation index (NDVI) change that does not vary significantly from one year to the next. We seek a set of pixels that is both spatially extensive and consists of pixels that, relative to other pixels in the scene, exhibit low-energy nonannual signal variation with respect to their NDVI values. Once identified, these pixels are used to determine interannual NDVI value drift.

In this paper, we first define the mathematical foundations and assumptions of our approach, demonstrate it on two areas commonly used as spectrally invariant targets for satellite sensor calibration, and then extend the methodology to the conterminous United States. Temporal averaging is used to separate different components of the temporal signal of a National Oceanic and Atmospheric Administration (NOAA) Advanced Very High Resolution Radiometer (AVHRR) NDVI time series into two major categories of information: the annual component attributable to periodic, seasonally driven changes in vegetation condition and the nonannual component, which actually consists of two elements: 1) interannual variation and 2) nonpersistent annual and subannual variation. The noise of the signal will be distributed into both components of the decomposition, unless it possesses unusual spectral characteristics. By removing the annual component, we deseasonalize the time series, and only the nonannual component remains. We assume that the interannual variation element of the nonannual NDVI component contains all information relevant to interannual NDVI value drift.

We intend to use the proposed decomposition to identify interannually stable pixels (relative to other pixels in the scene). Such pixels are generally associated with either ecologically stable regions or areas with reflectance characteristics that are largely weather-independent (such as pixels from unaltered urban areas or barren regions). The nonannual components of identified pixels will contain low energy relative to the nonannual components of other pixels in the study region. When this occurs, underlying interannual trends have an opportunity to present themselves pronouncedly in the nonannual component of the decomposition. The decomposition we propose allows us to statistically decouple the annual and nonannual components of our data.

II. Theoretical Analysis

A. Properties of Temporal Averaging

We begin with some definitions and notation. For any integers k and n, the Euclidean division algorithm guarantees that there exist unique integers q and r (the *quotient* and *remainder*, respectively) such that $n = qk + r$, where $0 \leq r < |k|$. Two integers j and k are said to be *congruent modulo* n (denoted $j \equiv k \bmod n$) if they return the same remainder in the division algorithm when dividing n by both numbers.

Let $X \in R^n, X = \{X(1), X(2), \ldots, X(n)\}$, be any real-valued, n-point time series. Let p be an integer such that $1 \leq p \leq n$. If we let E denote the expected value operator, then define time series S_p, for $1 \leq k \leq n$, by

$$S_p(k) = E(\{X(j) : j \equiv k \bmod p, 1 \leq j \leq n\}). \tag{1}$$

From (1), it is clear that S_p is a p-periodic n-vector, which means that $S_p(k) = S_p(k+mp)$ for all integers m such that $1 \leq k+mp \leq n$.

Let $\langle \cdot, \cdot \rangle$ denote the inner product on R^n. The following properties regarding S_p hold for arbitrary p and $n (1 \leq p \leq n)$:

1) $ES_p = EX$ (equality of 1st moments of X and S_p);
2) $\langle S_p, X - S_p \rangle = 0$ (S_p is orthogonal to its X complement);
3) $\langle X - \hat{X}, X - \hat{X} \rangle$, where $\hat{X}$ is p-periodic, is uniquely minimized when $\hat{X} = S_p$.

Manuscript received September 27, 2002; revised June 9, 2003. This work was supported in part by the National Aeronautics and Space Administration under Grant NAG5-11988.

J. H. Kastens and M. E. Jakubauskas are with the Kansas Biological Survey (KBS), University of Kansas, Lawrence, KS 66047 USA (e-mail: jkastens@ku.edu; mjakub@ku.edu).

D. E. Lerner is with the Mathematics Department, University of Kansas, Lawrence, KS 66045 USA (e-mail: lerner@math.ku.edu).

Digital Object Identifier 10.1109/TGRS.2003.817272

Property (3) says that the *sum of squared errors* (SSE) when approximating X by a p-periodic vector is minimized by S_p. Properties (1) and (2) can be verified by explicitly writing out the expressions and using the definition of S_p given in (1). To prove property (3), observe that we can partition the indices $1, 2, \ldots, n$ into equivalence classes modulo p (i.e., into subsets whose members are congruent modulo p). Now, since $\hat{X}$ is p-periodic, it is constant throughout each equivalence class subset of $\hat{X}$. Thus the unique SSE-minimizing value for this constant will be the mean value of the subset of X indexed by the equivalence class, which corresponds to our definition of S_p in (1).

Mathematically speaking, S_p is the projection of X onto the subspace of R^n containing p-periodic vectors. It is worth mentioning that if $n = qp$ (i.e., n is a multiple of p), then S_p equals the partial sum of Fourier harmonic components of X with fundamental frequencies that are multiples of q.

B. Decomposing NDVI Into Annual and Nonannual Components

In this paper we seek to decompose multiyear NDVI time series as NDVI $=$ (nonannual NDVI) $+$ (annual NDVI). For simplicity of notation, define $X_N =$ (nonannual NDVI) and $X_A =$ (annual NDVI), and so we have NDVI $= X_N + X_A$.

The decomposition we seek must satisfy the following three properties:

1) *Persistence:* X_A has yearly periodicity.
2) *Component Independence:* $\langle X_N, X_A \rangle = 0$.
3) *Maximum Energy Condition:* We require that the annual component X_A contains the maximum possible energy in the sense that $\langle Y_A, Y_A, \rangle \leq \langle X_A, X_A, \rangle \leq \langle \text{NDVI, NDVI} \rangle$ for any other decomposition NDVI $= Y_N + Y_A$ satisfying properties (1) and (2).

In light of property (2), property (3) is equivalent to requiring $\langle X_N, X_N \rangle \leq \langle Y_N, Y_N \rangle$ for any other decomposition NDVI $= Y_N + Y_A$ satisfying properties (1) and (2). Since $X_N =$ NDVI $- X_A$, this says that we want the X_A that minimizes the SSE when using X_A to approximate NDVI under the constraint of properties (1) and (2).

Comparing the above properties to the properties of S_p, it is clear that if we define $X_A = S_p$, where p is the number of points per year in the NDVI time series, then we will obtain the desired decomposition.

III. Empirical Analysis

A. Description of Data

The empirical component of this research uses AVHRR NDVI biweekly composite imagery covering the conterminous United States from the years 1990 to 2001. The imagery was obtained from the U.S. Geological Survey (USGS) EROS Data Center (EDC). Pixel resolution is 1 km $\times$ 1 km, and approximately 7.65 million terrestrial pixels comprise the study region (the conterminous United States).

NDVI is defined as NDVI $=$ (NIR $-$ RED)/(NIR $+$ RED), where NIR is reflectance (scaled to the range 0–255) in the near-infrared range (0.725–1.10 μm), and RED is reflectance (also scaled to the range 0–255) in the visible red range (0.58–0.68 μm) [5]. NDVI, which by definition takes values in the range $[-1, 1]$, is scaled by EDC to a range of 0–200 and rounded, allowing the data to be stored as eight-bit unsigned integers. The effective range of rescaled NDVI values associated with nonwater (terrestrial) areas is approximately 95–195. Nearly cloud-free AVHRR NDVI composites were created at EDC by extracting maximum NDVI values from individual NDVI images over a two-week period. The time step between each composited image is two weeks, giving 26 biweekly images per year. In order to obtain a temporally complete time series, missing images were interpolated from either temporally adjacent scenes or from the corresponding biweekly time period values from adjacent years (Table I). Thus, the final dataset for this study consists of a total of 312 images (26 images/year $\times$ 12 years).

TABLE I
Interpolated Images. Scenes Marked With an X Have Been Interpolated

Biweekly Time Period	1990	1991	1992	1993	1994	1995	2000	2001
1	X					X		X
2	X	X	X	X	X			X
3	X	X		X	X			X
4	X		X					
19					X			
20					X			
21					X			
22	X	X	X	X	X		X	
23					X		X	
24	X	X	X	X	X		X	
25					X		X	
26	X	X	X	X			X	

B. Empirical Results

After decomposing NDVI time series X as $X = X_N + X_A$, where $X_A = S_{26}$, we calculate $\langle X_N, X_N \rangle$ to obtain the amount of energy in signal X that we can attribute to nonannual variability. One of our hypotheses is that the pixels in a study region that possess the lowest values for this quantity are the most interannually stable pixels within that region.

The 48 states that form the conterminous United States comprise the region of study for the present analysis. We decomposed the time series for every pixel in each state as $X = X_N + X_A$, and then we calculated $\langle X_N, X_N \rangle$ for every pixel. The pixels within a state possessing the lowest values for $\langle X_N, X_N \rangle$ (i.e., the least energy in the nonannual component) compared to all other pixels in the state were selected as the most interannually stable and saved for analysis. This procedure led to the construction of a database consisting of 3493 pixel-level time series. This number was determined by allowing Rhode Island (the smallest state in geographic area) to contribute one pixel, and then allowing the other 47 conterminous states to contribute a number of pixels based on the proportion of their respective areas to the area of Rhode Island. For instance, Texas contributed 309 pixels to the database because the number of nonwater pixels in an AVHRR NDVI scene for Texas is approximately 309 times as many nonwater pixels in an AVHRR NDVI scene for Rhode Island. The time series obtained from averaging the time series associated with the 3493 selected pixels will be referred to as "US."

Time series from two known spectrally invariant targets (SITs) were used for validation. The first region is White Sands National Monument (hereafter denoted WS) in south central New Mexico, and the second is from the salt flats (hereafter denoted SF) southwest of Great Salt Lake in Utah. The WS time series was computed as the average time series of a 156-pixel block with upper left coordinates (106° 23′ 34″ W, 32° 54′ 35″) and lower right coordinates (106° 15′ 27″ W, 32° 49′ 7″ N). The SF time series was computed as the average time series from a 306-pixel block with upper left coordinates (113° 40′ 49 W, 40° 22′ 33″ N) and lower right coordinates (113° 27′ 8″ W, 40° 15′ 34″ N). In 52 of the 312 time periods, the spatial standard deviation of pixels contributing to the WS time series exceeded one NDVI, and the average spatial standard deviation across all time periods was 0.785 NDVI. For

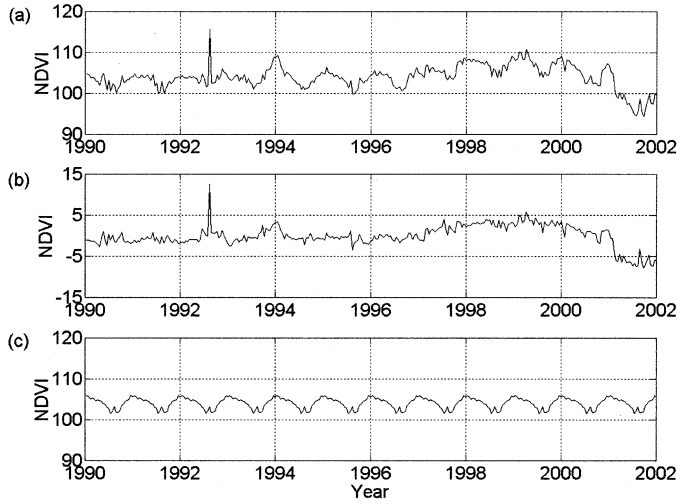

Fig. 1. (a) White Sands NDVI. (b) Nonannual component. (c) Annual component.

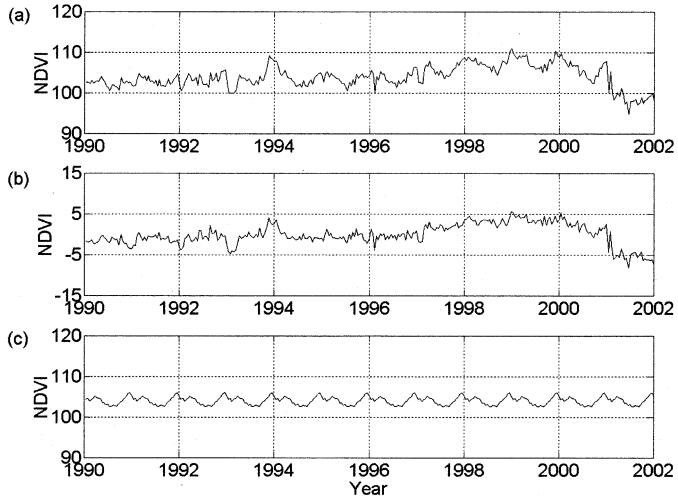

Fig. 2. (a) Salt flats NDVI. (b) Nonannual component. (c) Annual component.

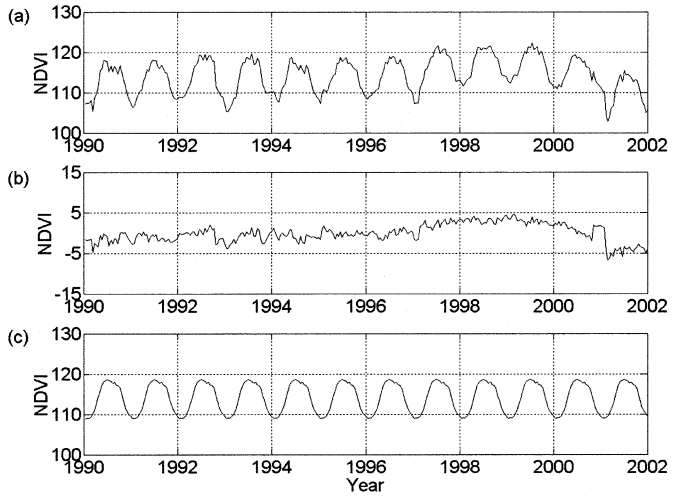

Fig. 3. (a) U.S. annually invariant pixel average NDVI. (b) Nonannual component. (c) Annual component.

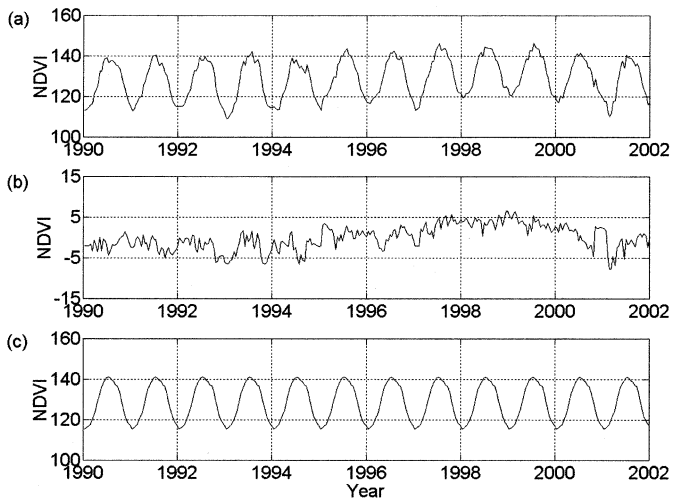

Fig. 4. (a) U.S. average NDVI (the CTRL time series). (b) Nonannual component. (c) Annual component.

SF pixels, 35 of the 312 time periods possessed a spatial standard deviation exceeding one NDVI, and the average spatial standard deviation across all time periods was 0.717 NDVI. Since the pixel-level NDVI values under investigation are integers, these numbers imply that spatial variability within each spectrally invariant target set was very low. The temporal standard deviation of the WS time series was 2.923, and the temporal standard deviation of the SF time series was 2.798. This variation, which is mostly seasonal, can be partly attributed to changes in solar zenith angle [7].

A control dataset (CTRL) was constructed from 3493 randomly selected pixels using the state-level area weighting described above. Given the large number of pixels contributing to this time series, only one such control is needed, as others derived the same way will be nearly identical. Furthermore, any time series generated in this fashion can be used as a highly accurate proxy to the all-pixel average time series (i.e., the average time series across all 7.65 million pixels in the study region).

The WS and SF time series, along with their respective annual and nonannual components, are shown in Figs. 1 and 2. Corresponding information from the US and CTRL time series is shown in Figs. 3 and 4, respectively.

The AVHRR NDVI time series used in this study consists of three regimes corresponding to different sensors that were used to collect the data. The first regime spans the years 1990–1994 and comprises data obtained using the NOAA-11 satellite. The second regime spans the years 1995 to 2000 and comprises data obtained using the NOAA-14 satellite. The third regime spans 2001 and comprises data obtained using the NOAA-16 satellite. As NDVI behavior can abruptly change when switching sensors (though it should not if the sensors are consistently calibrated), we seek three potential NDVI trend adjustments, one corresponding to each regime of the data.

Appropriate trend forms for the three data regimes were determined after inspecting the nonannual component of the US time series. A linear trend was sought for the first regime (NOAA-11, 1990–1994). A cubic trend was sought for the second regime (NOAA-14, 1995–2000), which exhibits nonlinear interannual behavior. As the third regime (NOAA-16, 2001) spans only one year, a constant shift was sought as the simplest possible trend adjustment. Fig. 5 shows the trends obtained from the nonannual components of the WS, SF, US, and CTRL time series, along with the SIT trend (an average of the WS and SF trends).

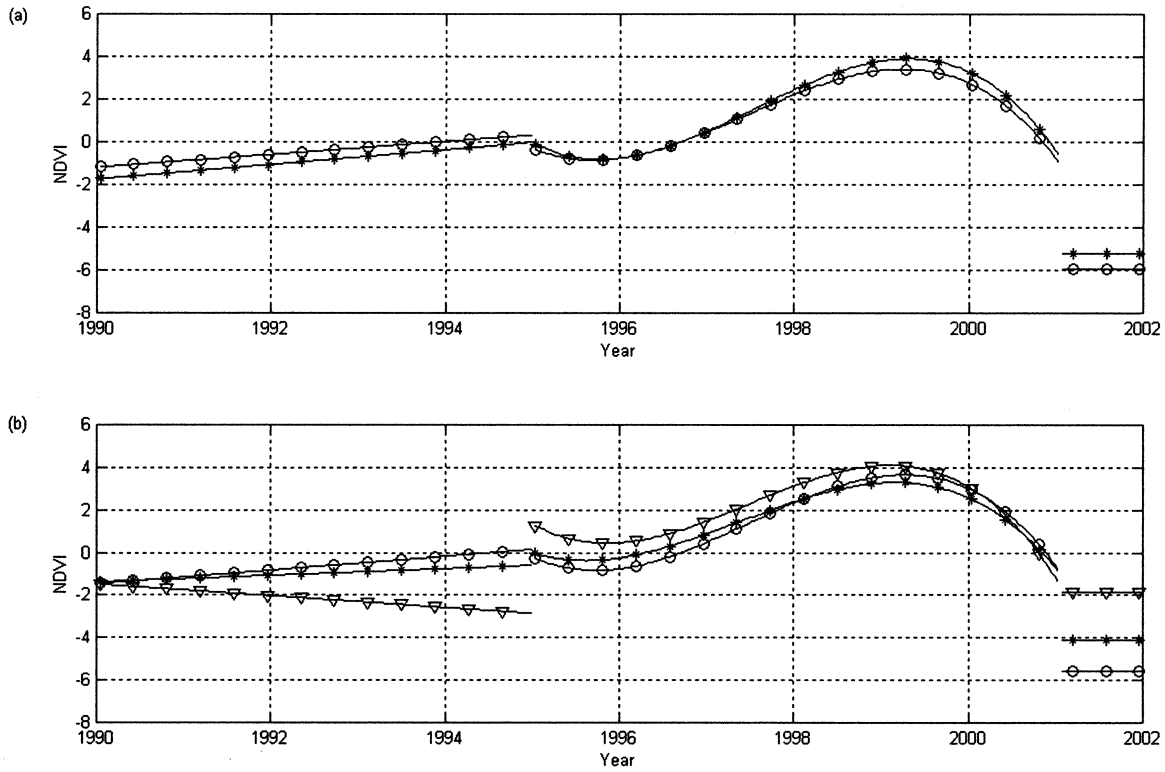

Fig. 5. (a) Spectrally invariant target NDVI trends ("∘" marks the WS trend, and "∗" marks the SF trend). (b) Other NDVI trends ("∘" marks the SIT trend, "∗" marks the US trend, and "▽" marks the CTRL trend).

The root-mean squared error (RMSE) between the US trend and the SIT trend is 0.5506, whereas the RMSE between the CTRL trend and the SIT trend is 1.6505. For comparison, the RMSE between the WS and SF trends is 0.4478. The R-squared value between the US trend and the SIT trend is 0.9527, whereas the R-squared value relating the CTRL trend to the SIT trend is 0.5516. The R-squared value between the WS and SF trends is 0.9617. A third measure of goodness-of-fit is mean absolute error (MAE). The MAE between the US trend and the SIT trend is 0.4268, whereas the MAE between the CTRL trend and the SIT trend is 1.3249. The MAE between the WS and SF trends is 0.3896. Neither the US trend nor the CTRL trend was biased away from the SIT trend, as both exhibited mean error on the order of 10^{-14} when differenced from the SIT trend.

C. Problems in the Source Bands

By definition, the NDVI data we are using is derived from information contained in the near-infrared (NIR) and red (RED) bands collected by the NOAA sensors. We receive this data from EDC in eight-bit unsigned integer format, so reflectance values have been scaled to the 0–255 range. NIR and RED data from 2000 and from the first three biweekly periods of 2001 are not included, as this information is not in our database. Fig. 6 shows values for the SIT time series derived from the NIR and RED bands. The flat lines in the graphs represent average values across the depicted temporal extents of the lines. In both bands, a large negative deviation from their respective 1990–1999 mean values is observed in 2001. The mean 2001 NIR value is more than 69 units (which is more than 3.67 standard deviations) below the 1990–1999 mean NIR value, whereas the mean 2001 RED value is over 44.6 units (more than 2.38 standard deviations) below the 1990–1999 mean RED value. The discrepancy between these 2001 value drops leads to a decreased value for the numerator (NIR−RED) in the NDVI formula. The value drops themselves lead to a decreased value in the denominator (NIR+RED) in the NDVI formula. Given the observed decline in 2001 NDVI baseline value, it follows that the numerator and denominator value declines are inconsistent with respect to computed NDVI.

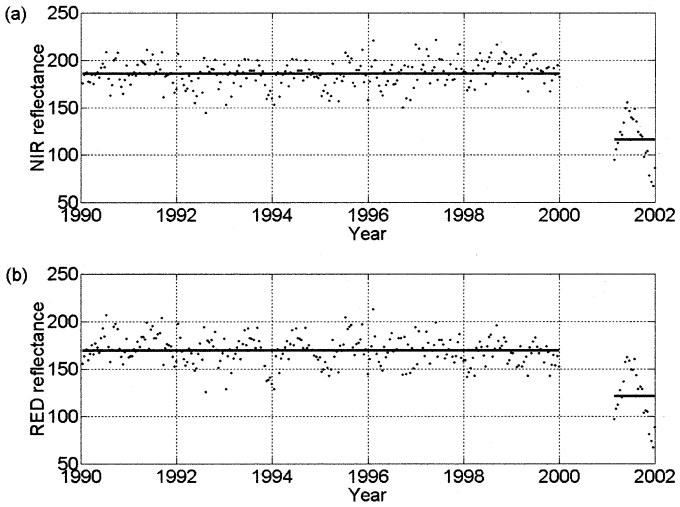

Fig. 6. (a) SIT NIR reflectance, scaled to 0–255. (b) SIT RED reflectance, scaled to 0–255. In both plots, the horizontal lines represent average values over the depicted temporal extents of the lines.

The USGS EROS Data Center was contacted to help determine the source of the discrepancies described above. EDC was able to determine that in the past (1989–2000) a solar zenith angle correction and an atmospheric correction for Rayleigh and ozone had been applied to the RED and NIR bands before calculating NDVI. In 2001, EDC began using NOAA-16 data and initiated a more stringent atmospheric correction that included correction for water vapor. Another trend analysis will be performed by the authors once we obtain from EDC a complete time series of water vapor corrected NDVI from 1990 to present.

D. Identifying Spectrally Invariant Targets

From the above analysis, we have evidence that the proposed pixel selection technique based on identifying pixels of minimum nonannual energy does in fact select SITs when they are available in the region of interest. By the area weighting technique previously described, New Mexico contributed 144 pixels to the 3493-pixel set used in the analysis. Referring to the USGS EDC map of Seasonal Land Cover Regions [8], New Mexico has two regions (White Sands, and a barren region near the northwest corner of the state) that stand out as the most spectrally invariant targets in the state. Ideally, most of the interannually stable pixels identified should come from these two areas and particularly from White Sands, since this is the better SIT candidate of the two. As discussed above, the WS time series was derived from 156 pixels lying entirely within White Sands. Of the 144 pixels selected using the proposed technique, 31 pixels were from the WS pixel set. If we include a five-pixel (5 km) buffer around the WS pixel set, along with the original WS pixels, then 79 of the 144 pixels lie within that region. Using a ten-pixel (10 km) buffer, the two pixels sets have 117 pixels in common. These findings indicate that the majority of pixels selected to represent interannually stable pixels from New Mexico fall within or in the immediate vicinity of White Sands.

IV. Conclusion

Our methodology using *annually invariant* targets for detection and quantification of sensor drift has significant advantages over previous approaches, particularly in circumstances where appropriate spectrally invariant targets for scene normalization or detection of sensor drift do not exist or cannot be reliably identified. The temporal averaging technique presented in this paper has obvious extensions beyond the realm of interannual NDVI trend analysis. The decomposition is applicable to any regularly sampled time series exhibiting a stationary periodicity whose period length is a multiple of the sampling period. The strength of the procedure in the present context lies in its ability to identify interannually stable pixels (with respect to NDVI time series) within a given scene.

Acknowledgment

The authors would like to thank J. Eidenshink (USGS EROS Data Center) for his help in identifying the primary source of the NDVI data inconsistencies addressed in this paper.

References

[1] P. Abel, G. R. Smith, R. H. Levin, and H. Jacobowitz, "Results from aircraft measurements over White Sands, New Mexico, to calibrate the visible channels of spacecraft instruments," in *Proc. SPIE, Recent Advances in Sensors, Radiometry, and Data Processing for Remote Sensing*, Orlando, FL, Apr. 6–8, 1988, pp. 208–214.

[2] D. I. Gellman, S. F. Biggar, M. C. Dinguirard, P. J. Henry, M. S. Moran, K. J. Thome, and P. N. Slater, "Review of SPOT-1 and -2 calibrations at White Sands from launch to the present," in *Proc. SPIE, Recent Advances in Sensors, Radiometric Calibration, and Processing of Remotely Sensed Data*, vol. 1938, 1993, pp. 118–125.

[3] B. L. Markham, J. R. Irons, D. W. Deering, R. N. Halthore, R. R. Irish, R. D. Jackson, M. S. Moran, S. F. Biggar, D. I. Gellman, B. G. Grant, J. M. Palmer, and P. N. Slater, "Radiometric calibration of aircraft and satellite sensors at White Sands, New Mexico," in *Proc. IGARSS*, Washington, DC, 1990, pp. 515–518.

[4] M. S. Moran, R. D. Jackson, T. R. Clarke, J. Qi, F. Cabot, K. J. Thome, and B. N. Markham, "Reflectance factor retrieval from Landsat TM and SPOT HRV data for bright and dark targets," *Remote Sens. Environ.*, vol. 52, pp. 218–230, 1995.

[5] A. P. Cracknell, *The Advanced Very High Resolution Radiometer*. Bristol, PA: Taylor & Francis, 1997.

[6] C. R. N. Rao, "Degradation of the Visible and Near Infrared Channels of the Advanced Very High Resolution Radiometer on the NOAA-9 Spacecraft: Assessment and Recommendations for Corrections," U.S. Dept. of Commerce, Washington, DC, NOAA Tech. Rep. NESDIS 70, 1993.

[7] R. K. Kaufmann, L. Zhou, Y. Knyazikhin, N. V. Shabanov, R. B. Myneni, and C. J. Tucker, "Effect of orbital drift and sensor changes on the time series of AVHRR vegetation index data," *IEEE Trans. Geosci. Remote Sensing*, vol. 38, pp. 2584–2597, Nov. 2000.

[8] T. R. Loveland, J. W. Merchant, B. C. Reed, J. F. Brown, D. O. Ohlen, P. Olsen, and J. Hutchinson, "Seasonal land cover regions of the United States," *Ann. Assoc. Amer. Geograph.*, vol. 85, no. 2, pp. 339–355, 1995.